JOURNAL OF SOLID STATE CHEMISTRY 52, 101–113 (1984)

Sm_2O_3–Ga_2O_3 and Gd_2O_3–Ga_2O_3 Phase Diagrams

J. NICOLAS, J. COUTURES, AND J. P. COUTURES[1]

Laboratoire des Ultra-Réfractaires, CNRS B. P. N° 5, Odeillo 66120, Font-Romeu, France

AND B. BOUDOT

Centre de Recherche Rhône Poulenc, 12/14, Rue des Gardinoux, 93308, Aubervilliers Cédex, France

Received March 23, 1983; in revised form October 11, 1983

Four definite compounds exist in the Sm_2O_3–Ga_2O_3 binary phase diagram, namely: Sm_3GaO_6, $Sm_4Ga_2O_9$, $SmGaO_3$, and $Sm_3Ga_5O_{12}$. The 3/1 compound is orthorhombic (space group *Pnna* – *Z*.4) with the cell parameters: $a = 11.40_0$ Å, $b = 5.51_5$ Å, $c = 9.07$ Å and belongs to the oxysel family. Sm_3GaO_6 and $SmGaO_3$ melt incongruently at 1715 and 1565°C; $Sm_4Ga_2O_9$ and $Sm_3Ga_5O_{12}$ have a congruent melting point at 1710 and 1655°C. With regard to the Gd_2O_3–Ga_2O_3 system three definite compounds have been identified: Gd_3GaO_6, $Gd_4Ga_2O_9$, and $Gd_3Ga_5O_{12}$. Only the garnet melts congruently at 1740°C with the following composition: $Gd_{3.12}Ga_{4.88}O_{12}$. Gd_3GaO_6, and $Gd_4Ga_2O_9$ melt incongruently at 1760 and 1700°C. $GdGaO_3$ is only obtained by melt overheating which may yield an equilibrium or a metastable phase diagram.

1. Introduction

The rare earth gallium garnets and single crystals of gadolinium gallium garnet (GGG) in particular are used as substrates for magnetic bubbles. This explains the number of papers on growing single crystals using the Czochralski technique. This technique was first explored by Linares (*1*), while specific aspects have been examined by Brandle (*2–4*), Heinz (*5*), and O'Kane (*6*). Another area of study concerns the nonstoichiometry of the garnet phase (Geller (*7*)) and stoichiometric comparison of single crystals and samples prepared using ceramic techniques (*8*).

In contrast to these studies, data concerning the equilibrium phase diagram for these systems is very scarce. Allibert *et al.* (*9*) have investigated the Gd_2O_3–Ga_2O_3 phase diagram between 0.40 and 0.80 Ga_2O_3 using mass spectrometry. More recently Diguiseppe *et al.* (*10, 11*) reexamined this portion of the diagram and came to the conclusion that, depending on the temperature of the melt, either equilibrium or nonequilibrium phase diagrams could be obtained. The hypothesis of Diguiseppe *et al.* is related to the fact that if $Sm_3Ga_5O_{12}$ or $Gd_3Ga_5O_{12}$ are heated to a temperature 80°C above their melting point, the liquid crystallizes as a mixture of perovskite and gallium oxide.

Four definite compounds of Ln_2O_3 and Gd_2O_3 have been identified. The gallium

[1] To whom correspondence should be addressed.

0022-4596/84 $3.00

garnet $Ln_3Ga_5O_{12}$ (cubic *Ia3d*) exists for *Ln* = Ce → Lu + Y with a nonstoichiometry range which increases as the Ln^{3+} radius decreases. The perovskite $LnGaO_3$ (orthorhombic *Pbnm*) is known for all the *Ln* elements (*12*). The 2/1 compound $Ln_4Ga_2O_9$ (monoclinic $P2_1/c$ (*13*) exists for *Ln* = La to Gd and a 3/1 (Ln_3GaO_6) phase was found for *Ln* = Sm and Gd by Schneider *et al.* (*15*) and Carruthers *et al.* (*16*). The perovskite $LnGaO_3$ can only be obtained by solid state reaction up to *Ln* = Nd. For *Ln* = Sm → Lu this technique yields the corresponding garnet $Ln_3Ga_5O_{12}$ and another phase dependent on the rare earth oxide and the annealing temperature. These perovskites have been obtained by decomposition of the corresponding garnet at high pressure (45 kbars) and at a temperature of around 1000°C, using NaOH flux. Pure perovskites are obtained for *Ln* = Sm → Tb, whereas for *Ln* = Dy → Lu, decomposition of the garnet is only partial (Marezio *et al.* (*12*)). More recently, Geller *et al.* (*17*) obtained these perovskites for *Ln* = Sm → Er after overheating the 0.5 Ln_2O_3–0.5 Ga_2O_3 liquid mixture. A precise and careful determination of the Ln_2O_3–Ga_2O_3 phase diagram is required if the problem is to be fully understood. This paper reports the results obtained in our study of the Sm_2O_3–Ga_2O_3 and Gd_2O_3–Ga_2O_3 phase diagrams.

2. Experimental

The purity of the oxides supplied by Rhône-Poulenc were Ga_2O_3 4 *N*, Sm_2O_3 and Gd_2O_3 3 *N*. Prior to use they were annealed at 1200°C for 5 hr in order to remove anionic impurities. The samples were prepared in air using three different methods:

—Solid state reaction up to 1600°C of appropriate mixtures of the starting oxides;

—Solid state reaction over the same temperature range of intimate mixtures, using the process described by Allibert *et al.* (*9*);

—Comelting of mixtures of the starting oxides, using a laboratory-scale solar furnace (*18*) or a special device associated with a CO_2 laser.

Phase identification of all samples was undertaken using room-temperature X-ray diffraction (Fe$K\alpha$ radiation—goniometer scanning speed 1°/min in 2θ).

Our findings confirmed the assertion of Carruthers *et al.* (*16*) that with 3 : 5 Gd_2O_3–Ga_2O_3 the low reactivity of the oxide mixtures prevents an equilibrium state being reached even after prolonged annealing (200 hr). In consequence the "citric complex" method previously described (*9*) was employed. The correct amounts of Gd_2O_3 and Ga_2O_3 were dissolved in nitric oxide. After the nitrates were obtained, citric acid was added and the solution evaporated to a transparent, viscous syrup. The syrup was then slowly decomposed and the resulting powder heated to 1200°C for 20 hr and 1600°C for 3 hr before being quenched.

Fusion of oxide mixtures was achieved using a 2-kW vertical axis solar furnace and a technique previously described (*18*). Because of the high rate of vaporization of Ga_2O_3, the melting time was limited to 15 sec. The use of a water-cooled copper plate as sample holder and the characteristics of the solar concentrator induce temperature gradients both on the surface and inside the sample; these prevent formation of metastable perovskite even at surface temperatures which are 200°C higher than the liquidus temperature, as Diguiseppe *et al.* (*10, 11*) already noted. Overheating without such a high temperature gradient was achieved using the apparatus shown in Fig. 1. Heating is provided by a CW CO_2 laser (1) (λ = 10.6 μm–*P* = 500 W). The laser beam (3) falls via a reflecting mirror (2) on the sample holder (4) containing the sample. This iridium crucible is placed on a hollow cylinder of stabilized zirconia (6), supported by a stainless-steel plate (7), and a water-cooled plate (9). The crucible is sur-

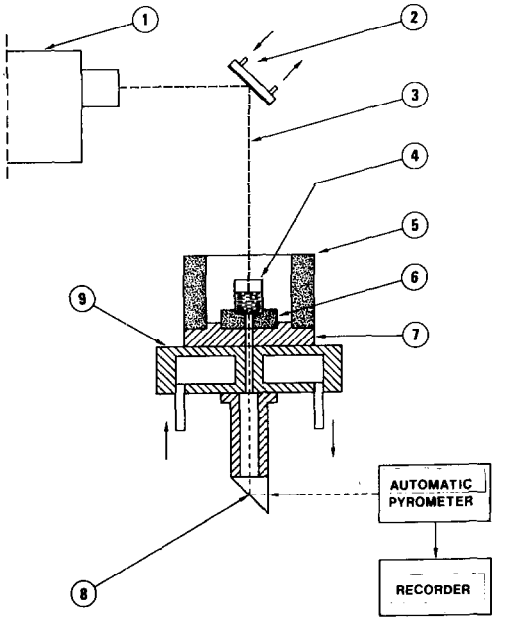

FIG. 1. Melting device associated with a CW CO_2 laser.

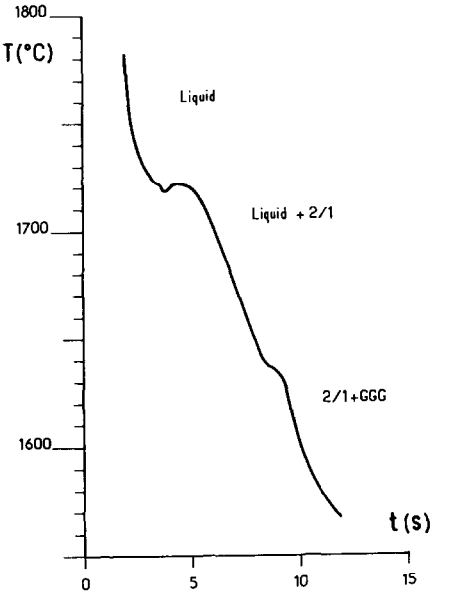

FIG. 2. Cooling curve (via the solar thermal analysis device) of a 0.625 Gd_2O_3 mixture.

rounded by radiation shields in stabilized zirconia (5). A prism (8) enables temperature to be measured at the bottom of the crucible. Pure metastable perovskite may thus be obtained.

The liquidus and solidus lines were drawn from the results obtained using different thermal analysis devices. The first one, previously described (*19*), is associated with a 2-kW horizontal axis solar furnace. The temperature is measured with an optical pyrometer under good blackbody conditions (*20*) (λ pyrometer = 0.810 μm—practical emissivity ~0.99). The cooling curve of a 0.625 Gd_2O_3 mixture is shown in Fig. 2, as an example. In the temperature range 1400–1700°C, such a technique is not suitable for thermal arrests at intervals of a few degrees. This was observed during investigation of the Sm_2O_3–Ga_2O_3 phase diagram in the 0.5 Ga_2O_3 region. Here the apparatus shown in Fig. 3 is used. In this furnace a lanthanum chromite heating element surrounds the alumina tube (3). The sample holder (5) is made of platinum. Two Pt–PtRh1% thermocouples are used. Thermocouple (1) is used for temperature programming. Sample temperature is mea-

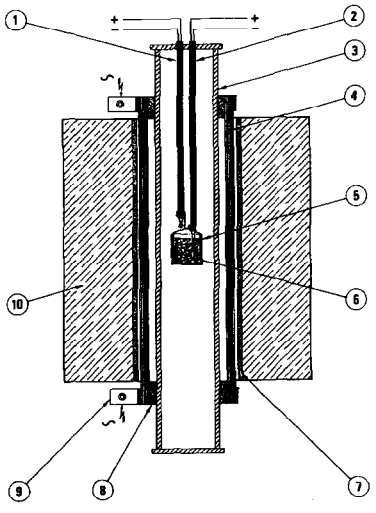

FIG. 3. Thermal analysis device associated with a $LaCrO_3$ furnace.

sured by thermocouple (2), the extremity of which is immersed in the sample (6). The radiation shields (7, 8) are of alumina, while the furnace insulation (10) is made from alumina wool. The hot zone extends over 30 mm, with a temperature homogeneity of ±5°C. The temperature is programmed linearly versus time. The signal of thermocouple (2) is received by a 2-channel high impedance recorder either directly (channel 1) or as a derivative (*dEmV/dt*—channel 2). Two cooling processes were used; typical results are shown in Fig. 4. The temperature measurements, expressed in the 68 IPTS, are correct to ±10°C, with the solar thermal analysis apparatus, and to ±3°C with the thermocouple.

3. Results

The two systems were scanned over the Ga_2O_3 composition range of 0.1–0.8 in 5% mole steps, either by solid state reaction or by melting.

3.1. Definite Compounds

Four definite compounds were identified, namely: 3/1, 2/1, 1/1, and 3/5, thus confirming the available published data. Sm_3GaO_6 and Gd_3GaO_6 do not melt congruently. They are stable from 1000°C up to the peritectic temperature (1745°C for Sm_3GaO_6 and 1760°C for Gd_3GaO_6). These compounds are isostructural to Nd_3GaO_6. A structural study of this compound (*21*) showed that the cell is orthorhombic (space group *Pnna*) with four units per cell. Optical data on Nd_3GaO_6 (*21*) show that these compounds belong to the oxysel family with a Ln^{3+} coordination number of around 7. The orthorhombic cell parameters are

Sm_3GaO_6: $a = 11.40_0$ Å, $b = 5.51_5$ Å,
$c = 9.07$ Å, $V = 570.2$ Å^3

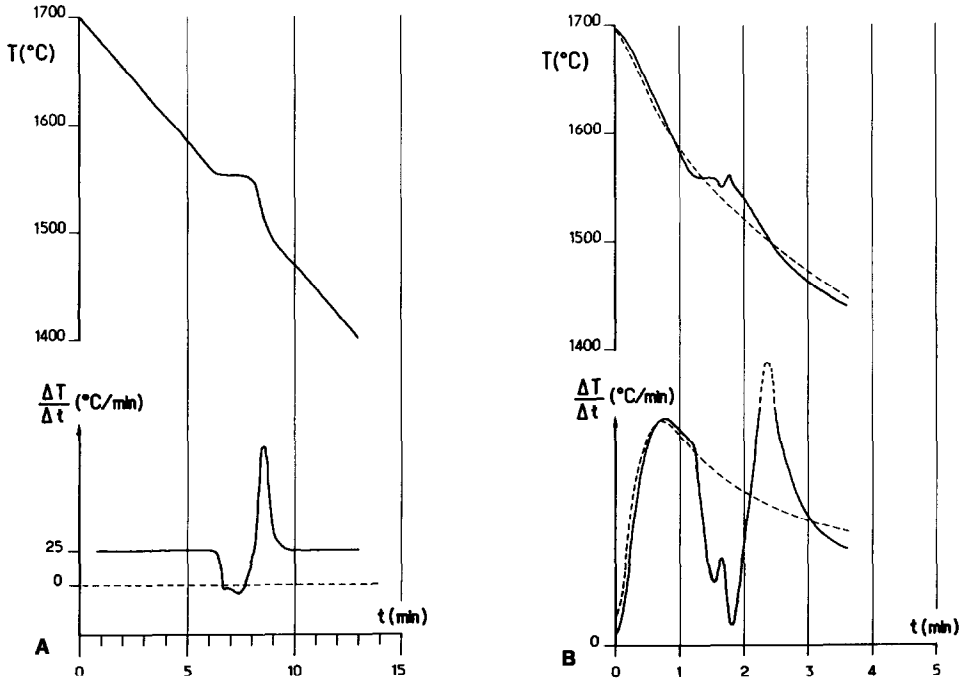

FIG. 4. Cooling curves and their derivatives of a 0.5 Sm_2O_3 mixture (dashed lines cooling process of the empty crucible). (A) Cooling speed 25°C min^{-1}. (B) Natural cooling of the furnace.

Gd_3GaO_6: = 11.27_8 Å, $b = 5.48_0$ Å, $c = 8.99$ Å, $V = 555.6$ Å^3

No variation in the cell parameters was detected around the 3/1 composition, showing that this compound is stoichiometric. In Table I is specified the indexing of Sm_3GaO_6 (this sample was melted and annealed at 1400°C for 24 hr after appropriate grinding). $Sm_4Ga_2O_9$ has a congruent melting point at 1705°C and decomposes below 1300°C; $Gd_4Ga_2O_9$ melts incongruently at 1700°C and is stable above 1490°C. These compounds are isostructural with $Eu_4Al_2O_9$ (monoclinic $P2_1/c$ – $Z = 4$ (*13*). In the structure the Al^{3+} ions are fourfold coordinated, with O–Al–O angles of between 98 and 121°; two of the Ln^{3+} ions are sixfold coordinated; and the two others sevenfold coordinated. The cell parameters are

$Sm_4Ga_2O_9$: $a = 7.68_5$ Å, $b = 10.89_0$ Å, $c = 11.42_5$ Å, $\beta = 108°75$

$Gd_4Ga_2O_9$: $a = 7.56_1$ Å, $b = 10.78_3$ Å, $c = 11.41_2$ Å, $\beta = 108°49$

The 2/1 compound is stoichiometric because no variation of the cell parameters occurs for samples prepared close to the 2/1 composition. The indexation of $Gd_4Ga_2O_9$, previously melted ground and annealed at 1550°C for 6 hr, is given in Table II.

$SmGaO_3$ melts incongruently at 1565°C and only exists over a small temperature range (~20–30°C below the liquidus temperature). Several attempts to obtain

TABLE I

INDEXATION OF Sm_3GaO_6 X-RAY POWDER PATTERNS[a]

hkl	I_{obs}	*d* calc (Å)	*d* obs (Å)
111	20	4.3548	4.3537
210	12	3.9635	3.9623
202	8	3.5488	3.5466
301 } 012 }	8	3.5048 3.5028	3.5035
212	100	2.9843	2.9843
311	60	2.9580	2.9580
103	26	2.9223	2.9220
400	22	2.8500	2.8492
020	30	2.7575	2.7570
113	12	2.5822	2.5829
121	6	2.5703	2.5702
410	8	2.5319	2.5317
220	2	2.4823	2.4826
303	5	2.3659	2.3657
004	7	2.2675	2.2670
412	8	2.2107	2.2108
222 } 313 }	8	2.1774 } 2.1742 }	2.1747
123	34	2.0056	2.0059
420	25	1.9817	1.9818
214	6	1.9682	1.9686

[a] Orthorhombic: $a = 11,40_0$ Å, $b = 5,51_5$ Å, $c = 9.07$ Å.

TABLE II

INDEXATION OF $Gd_4Ga_2O_9$ X-RAY POWDER PATTERNS[a]

hkl	I_{obs}	*d* calc (Å)	*d* obs (Å)
002	6	5.4122	5.4174
012	25	4.8357	4.8378
11$\bar{2}$	9	4.6704	4.6704
120	4	4.3093	4.3142
022	8	3.8197	3.8197
013	70	3.4216	3.4216
22$\bar{1}$	100	3.0947	3.0988
023	100	2.9980 }	2.9965
211	90	2.2973 }	
131	20	2.9670	2.9662
004	6	2.7060	2.7060
040	30	2.6956	2.6937
202	30	2.6295	2.6290
041	4	2.6157	2.6157
20$\bar{4}$	40	2.5908	2.5902
211	10	2.5543	2.5554
033	20	2.5462	2.5473
123	15	2.5381	2.5397
12$\bar{4}$	14	2.5179	2.5190
231	5	2.3566	2.3566
23$\bar{3}$	5	2.3376	2.3358
015 } 232 }	25	2.1224 } 2.1220 }	2.1220

[a] Monoclinic: $a = 7.56_1$ Å, $b = 10.78_3$ Å, $c = 11.41_2$ Å, $\beta = 108°49$.

$SmGaO_3$ by solid state reaction, at temperatures up to 1500°C, using mixed powders or coprecipitated materials, were unsuccessful. Nevertheless the perovskite was observed, for samples melted with the solar furnace and quenched at a cooling rate of around 250°C · sec^{-1}, over a composition range of 0.40–0.475 Ga_2O_3. With $GdGaO_3$, these techniques have never produced the perovskite, even as a trace. Nevertheless, short meltings and overheating of the melt using the laser device yield pure $SmGaO_3$ and $GdGaO_3$. These perovskites are isostructural with $GdFeO_3$ (space group *Pbnm* − $Z = 4$ (*22*)). Their parameters are

$SmGaO_3$: $a = 5.36_9$ Å, $b = 5.52_0$ Å, $c = 7.65_0$ Å, $V = 226.7$ Å^3

$GdGaO_3$: $a = 5.32_0$ Å, $b = 5.52_9$ Å, $c = 7.60_1$ Å, $V = 223.6$ Å^3

Our cell parameters are in good agreement particularly with the data of Marezio *et al.* (*12*) ($SmGaO_3$: $a = 5.36_9$ Å, $b = 5.52_0$ Å, $c = 7.65_0$ Å; $GdGaO_3$: $a = 5.322$ Å, $b = 5.537$ Å, $c = 7.606$ Å), but differ slightly from results by Geller *et al.* (*17*) ($SmGaO_3$: $a = 5.377$ Å, $b = 5.513$ Å, $c = 7.654$ Å; $GdGaO_3$: $a = 5.325$ Å, $b = 5.535$ Å, $c = 7.607$ Å). There is no doubt that these phases are identical; nevertheless, the differences could be due to the range of reflexion angles used in our cell parameters calculation $28 \leq 2\theta \leq 80$ (Fe$K\alpha$) in comparison with $35 \leq 2\theta \leq 170$ (Cr$K\alpha$) by Marezio *et al.* and $130 \leq 2\theta \leq 160$ (Cr$K\alpha$) by Geller *et al.*

The SmGG and GGG are stable up to their melting points of 1655 and 1740°C (±10°C), respectively, and exhibit nonstoichiometry. For samples melted with the solar furnace and quenched at 250°C. sec^{-1}, the cubic cell parameter of the first garnet varies from $a = 12.43_2$ Å (0.625 Ga_2O_3) to $a = 12.50_0$ Å (0.475 Ga_2O_3 which is a biphasic mixture of SmGG and $Sm_4Ga_2O_9$). Between 0.40 and 0.475 Ga_2O_3, three phases are observed on fused samples namely $Sm_4Ga_2O_9$, $SmGaO_3$, and SmGG, the garnet having a constant cell parameter equal to 12.50_0 Å. With the same synthesis process the GGG cell parameter varies from $a = 12.37_5$ Å (0.625 Ga_2O_3) to $a = 12.49_5$ Å (0.56 Ga_2O_3), as shown in Fig. 5. Annealing at different temperatures, of mixtures of the starting oxide in the Ga_2O_3 composition range 0.35–0.70 (Fig. 6), yields results that lead to the same conclusion reached by Carruthers *et al.* (*16*). The equilibrium state is not reached after an annealing time of 24 hr at 1300°C or 3 hr at 1600°C. The garnet cell parameter continues to increase in the biphasic region: Gd_3GaO_6 + GGG_{ss} at 1300°C and $Gd_4Ga_2O_9$ + GGG_{ss} at 1600°C. With a 0.58 Ga_2O_3 mixture the garnet parameter increases even after a 200-hr anneal at 1300°C. The equilibrium state is only reached if coprecipitation techniques are

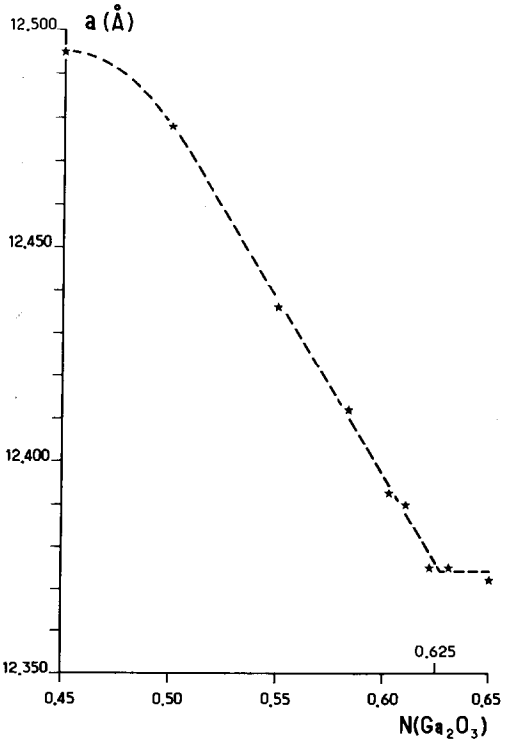

FIG. 5. Variation of the GGG_{ss} cell parameter of melted samples versus composition.

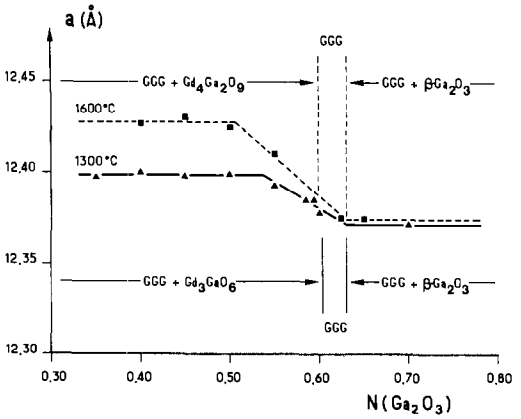

FIG. 6. Variation of the GGG_{ss} cell parameter on samples obtained by solid state reaction versus composition: annealing time 1300°C—24 hr, 1600°C—3 hr).

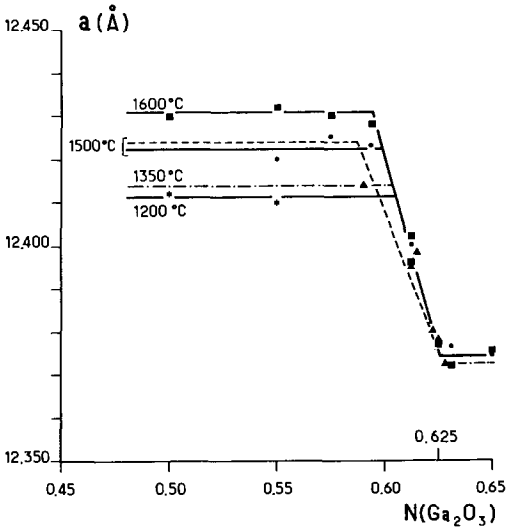

FIG. 7. Change versus the composition of a GGG_{ss} on samples obtained by solid state reaction of coprecipitated materials after annealing at different temperatures. (—) Our results (citric cmplex);(---) Allibert *et al.* (*9*) data; (·---) Rhône-Poulenc Research Center results (*22*).

used. The results are presented in Fig. 7. Our data, obtained using the citric complex method, is compared with the Allibert *et al.* results (*9*) for the same elaboration process and with the results obtained by one of our colleagues at the Rhône Poulenc Research Center (*23*). Rhône-Poulenc's data is in close agreement with Allibert's results. When a biphasic region is reached no variation of the garnet cell parameter is observed. The cell parameter and the composition of the GGG limit solid solution on the Gd_2O_3-rich side are presented for some temperatures in Table III.

3.2. Phase Diagram

Figure 8 lists the different phases observed for samples prepared by different processes versus N (Ga_2O_3) for the Sm_2O_3–Ga_2O_3 binary system (Table IV). Preparation techniques comprise solid state reaction of mixtures of the starting oxides after 24 hr, annealing at 1200 and 1400°C, and melting of materials using the solar furnace. The figure shows that

—The 3/1 compound has a noncongruent melting point;

—The 2/1 compound melts congruently and is only obtained above 1200°C;

—The 1/1 perovskite is decomposed during melting and is not obtained by solid state reaction up to 1400°C;

—The SmGG garnet has a congruent melting point;

—Three eutectics exist on the liquidus curve.

The X-ray powder patterns obtained on the Sm_2O_3- and β-Ga_2O_3-rich side indicate that there is no solubility of Ga^{3+} ions in Sm_2O_3 and of Sm^{3+} ions in β-Ga_2O_3. This

TABLE III

LIMIT OF THE GGG SOLID SOLUTION ON THE Gd_2O_3-RICH SIDE VERSUS TEMPERATURE

T (°C)	Cell parameter (Å)	Composition N (Ga_2O_3)
1200	12.411	0.605
1350	12.414	0.603
1500	12.422	0.598
1600	12.431	0.594
1640[a]	12.495	0.558

[a] 2/1—GGG eutectic line.

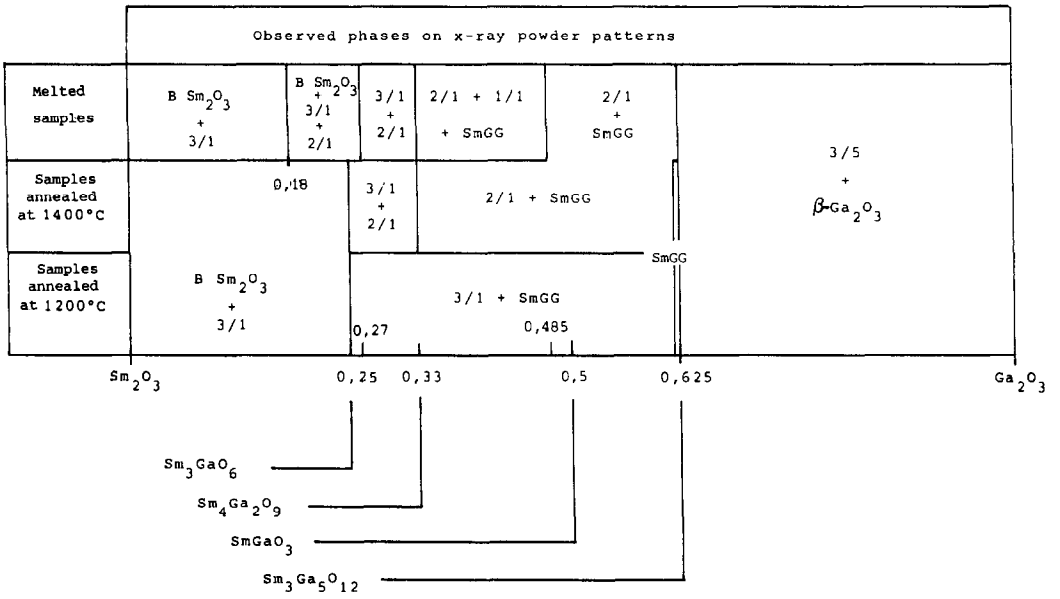

FIG. 8. Nature of the observed phase in the Sm_2O_3–Ga_2O_3 binary system versus composition and synthesis processes.

fact is related to the difference in the ionic radii of Ga^{3+} and Sm^{3+}, which, according to Shannon and Prewitt (*24*), are, respectively, $r(Ga^{3+}_{IV}) = 0.47$ Å, $r(Ga^{3+}_{VI}) = 0.62$ Å, and $r(Sm^{3+}_{VI}) = 0.96_4$ Å. The phase diagram is shown in Fig. 9, using the two thermal analysis devices mentioned above, in the Ga_2O_3 range 0.40–0.625. The diagram shows that the perovskite only exists over a limited temperature range, from approximately 1545 to 1565°C.

TABLE IV

INVARIANT POINTS ON THE LIQUIDUS CURVE OF THE Sm_2O_3–Ga_2O_3 PHASE DIAGRAM

N (Ga_2O_3)	T(°C) at ±10°C	Nature of the invariant point
0.27	1715	Peritectic decomposition of the 3/1 compound
0.30	1695	3/1–2/1 eutectic
0.333	1710	$Sm_4Ga_2O_9$ congruent melting poin
0.475	1555[a]	2/1–1/1 eutectic
0.485	1565[a]	Peritectic decomposition of the 1/1 compound
0.625	1655	$Sm_3Ga_5O_{12}$ congruent melting point
0.77	1540	SmGG–β-Ga_2O_3 eutectic

[a] At ±5°C.

For the Gd_2O_3–Ga_2O_3 binary phase diagram, the different phases observed on samples obtained either by solid state reaction or by melting are shown in Fig. 10. This figure shows that

—Only the garnet compounds have a congruent melting point;

—The existence of four phases in the composition range 0.225–0.275 implies the presence of two adjacent peritectics;

—The 2/1 compound is stable only at high temperatures ($T > 1490$°C) and melts incongruently;

—Two eutectics are observed on the liquidus curve.

For this system also, due to the large difference in ionic radii ($rGd^{3+}_{VI} = 0.938$ Å), no dissolution of Gd^{3+} in β-Ga_2O_3 or of Ga^{3+} in Gd_2O_3 was observed. The phase diagram is given in Fig. 11. The invariant points of

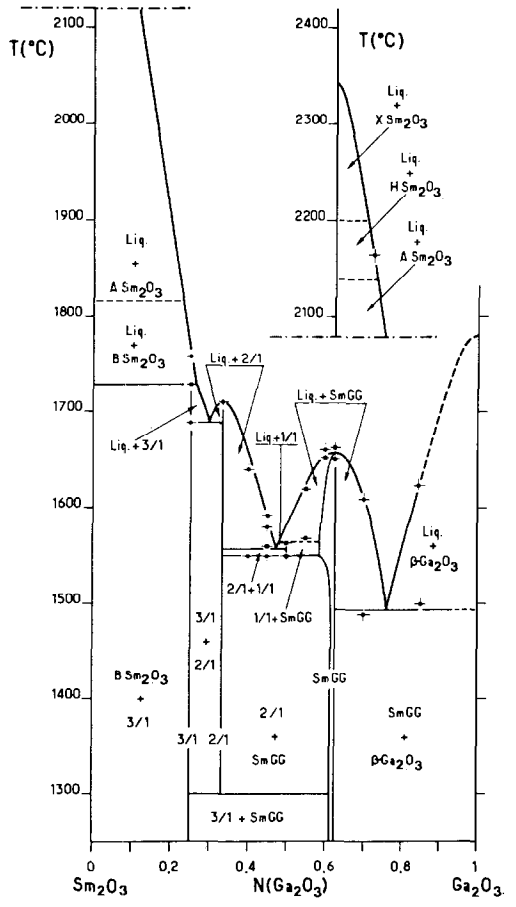

FIG. 9. Sm_2O_3–Ga_2O_3 phase diagram.

the liquidus curve are shown in Table V. A large number of thermal analyses have been carried out on samples in the Ga_2O_3 composition range 0.55–0.65, showing that congruent melting occurs at 0.61 Ga_2O_3, in close agreement with the result of Allibert *et al.* (*9*).

4. Discussion

4.1. Garnet Stoichiometry

As previously noted, the experimental results concerning the GGG show that the solid solution extended to the Gd_2O_3-rich side. Under equilibrium conditions the variation of the cell parameter obeys Vegard's law. Figures 5 and 6 show a linear relationship between a_{GGG} and $N(Ga_2O_3)$; nevertheless this could not be used for the determination of the GGG nonstoichiometry range because a_{GGG} increases in the biphasic region. Such a behavior indicates that the sample has not reached the equilibrium state. For this reason Figs. 5 and 6 also could not be used for determining the range of existence of GGG. Figure 7 is based on samples which have reached their equilibrium state (coprecipitated techniques). The composition of the limit of the solid solution could be obtained by the intersection of the Vegard line and the line of constant parameter, using the highest value found for a_{GGG} (a = 12.495 Å on melted samples). This figure establishes the limit of Gd_2O_3 solubility in the GGG cell parameters versus the temperature as shown in Table III.

According to the Geller (*7*) hypothesis, with direct substitution of hexacoordinated Ga^{3+} by Ln^{3+}, the formula of the garnet corresponding to the highest Gd^{3+} solubility is Gd_3 $(Gd_{0.52}Ga_{1.48})$ Ga_3O_{12}. In the case of SmGG, the cell parameter variation is too small for precisely establishing the Vegard line. The highest Sm^{3+} solubility in the SmGG could thus not be accurately determined. Thus, we used the model described by Brandle and Barns (*8*), which uses the Geller hypothesis to calculate the degree of departure from the stoichiometry of grown crystals. This model was extended to the whole range of garnet stoichiometry and permits the composition x to be established in the garnet formula $Ln_3(Ln_xGa_{2-x})Ga_3O_{12}$, as well as the difference, Δa_0, between the cell parameters of the nonstoichiometric and the stoichiometric garnet. The Vegard line equation for GGG is x = 3.894 Δa_0, which leads to an x value of 0.467 for the limit of the solid solution. This value corresponds to a composition of 0.566 Ga_2O_3, which is in close agreement with the experimental data (Fig. 7, Table III: 0.56 Ga_2O_3). As applied

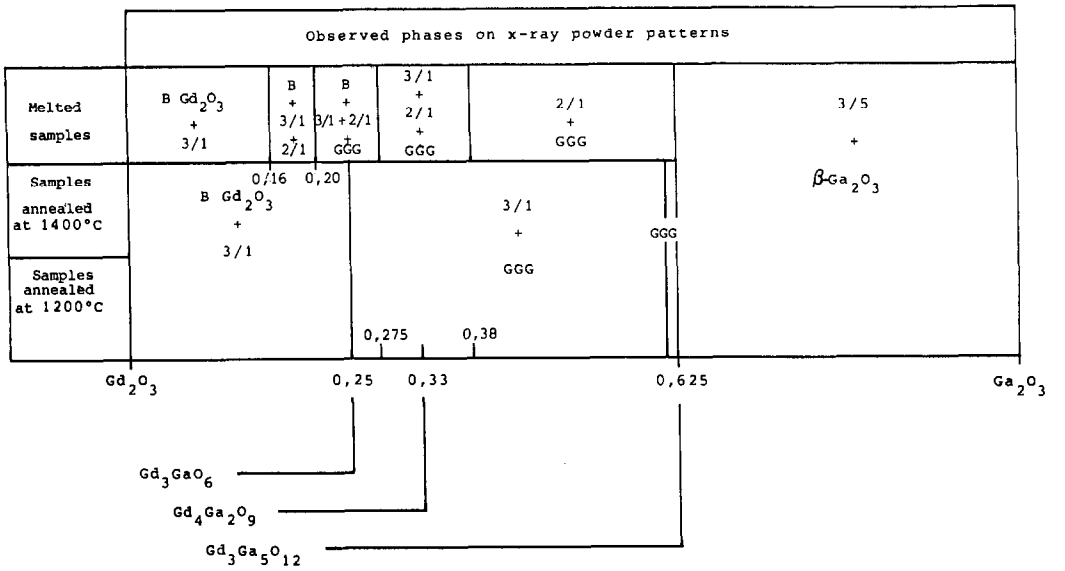

FIG. 10. Nature of the observed phase in the Gd_2O_3–Ga_2O_3 binary system versus the composition and the synthesis processes.

to SmGG, the Vegard line equation is $x = 3.6\,\Delta a_0$, with a limiting solid solution of $x = 0.245$ ($Sm_3[Sm_{0.245}Ga_{1.755}]Ga_5O_{12}$), corresponding to $N(Ga_2O_3) = 0.594$.

4.2. *Melt Temperature Relationship for $3Ln_2O_3$–$5Ga_2O_3$ Liquids*

Gillissen *et al.* (*25*) and Caslavsky *et al.* (*26*) have shown that if $Dy_3Al_5O_{12}$ and $Y_3Al_5O_{12}$ are heated above their melting points, crystallization leads to a single phase garnet or to a mixture of perovskite and aluminum oxide α-Al_2O_3, depending on the maximum temperature reached by the melt. The strange behavior of this type of liquid was also observed by Diguiseppe *et al.* (*10*) for $Sm_3Ga_5O_{12}$ and $Gd_3Ga_5O_{12}$. This behavior could be related to the existence of a critical temperature T_C in these liquids. If $\Delta T = T_C - T_f$, where T_f is the garnet melting point, ΔT is equal to 15°C for $Y_3Al_5O_{12}$ and to 70–80°C for $Sm_3Ga_5O_{12}$ and $Gd_3Ga_5O_{12}$. We believe that these results are due to a change in the oxygen nearest neighbors of the cations in the liquid. If we consider that $\Delta T \approx 70$–80°C for gallium garnets and only 15°C for yttrium aluminium garnet, the low value for the latter compound is consistent with the fact that Al^{3+} forms the sixfold coordination more readily than does Ga^{3+}. The fact that crystallization of a liquid heated to a temperature above T_C produces a perovskite phase in which the Al^{3+} or Ga^{3+} coordination number is 6 and the Ln^{3+} coordination number around 12,

TABLE V

INVARIANT POINTS ON THE LIQUIDUS CURVE OF THE Gd_2O_3–Ga_2O_3 PHASE DIAGRAM

$N(Ga_2O_3)$	T (°C) ± 10°C	Nature of the invariant point
0.275	1760	Peritectic decomposition of the 3/1 compound
0.38	1700	Peritectic decomposition of the 2/1 compound
0.46	1640	2/1-GGG eutectic
0.61	1740	GGG_{ss} congruent melting point
0.78	1580	GGG–β-Ga_2O_3 eutectic

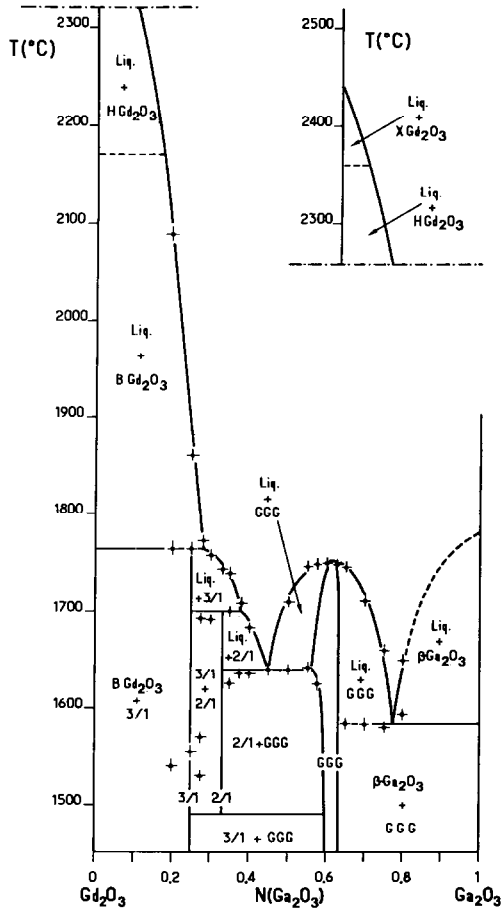

FIG. 11. Gd_2O_3–Ga_2O_3 phase diagram.

implies that at T_C the liquid structure changes.

The changes by overheating are observed only in the absence of garnet phase nucleating agents. Globules with the GGG composition have been melted on a water-cooled copper plate at the focus of a 2-kW vertical axis solar furnace. Even though the globule surface was heated nearly 250°C above the melting point, a single garnet phase always crystallized. The reason is that the temperature of the bottom of the globule which is supported by the cooled plate is not above T_C. During cooling, GGG crystallizes first, and this nucleates crystallization of this phase for the whole globule. Only devices ensuring homogeneity of the high temperature melt permits the metastable perovskite phase to be observed when the temperature of the liquid is above T_C. These results show that care must be taken to avoid mistaking the metastable phase for the equilibrium phase or including elements from both phases in the same diagram. The diagram by Allibert *et al.* (*9*) is an example; as Fig. 11 shows no break occurs at 0.5 Gd_2O_3 on the liquidus line. In addition, $GdGaO_3$ has never been obtained except with the CO_2 laser device when the melt is overheated to near 1900°C. We believe that the observation by Allibert *et al.* of the perovskite is strictly related to the heating device and to the fact that, for perovskite composition, the temperature of the melt prior to thermal analysis was above T_C. Figure 12 shows the equilibrium phase diagram (our results) and the metastable diagram using data by Allibert *et al.* and Diguiseppe *et al.* Such a metastable phase diagram could never have been drawn with our thermal analysis apparatus associated with a solar furnace because the liquid is surrounded by a solid causing the stable phase to crystallize. Insufficient data are at presently available to determine the variation of T_C with melt composition, although this determination is under study.

5. Conclusion

Equilibrium phase diagrams of the Sm_2O_3–Ga_2O_3 and Gd_2O_3 binary systems have been drawn. Four definite compounds have been identified, namely: Ln_3GaO_6, $Ln_4Ga_2O_9$, $LnGaO_3$, and $Ln_3Ga_5O_{12}$, except for the case of Gd where the perovskite is only obtained if the melt is overheated in an iridium crucible above the critical temperature T_C. In the absence of stable-phase nucleating agents, this critical temperature of the liquid could result in the drawing of a metastable phase diagram. A model based on the Geller hypothesis with regard to sub-

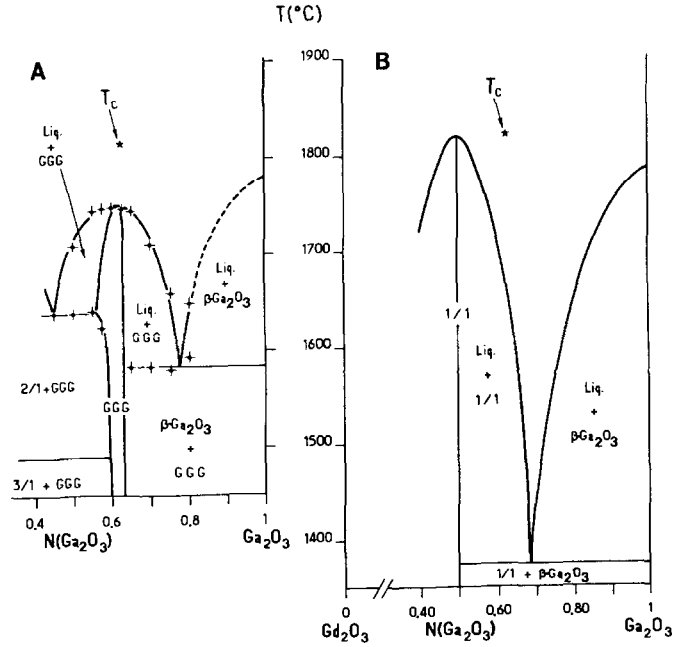

FIG. 12. Stable and metastable phase diagram for the Gd_2O_3–Ga_3O_3 binary system in the Ga_2O_3 range 0.4–1. (A) Equilibrium phase diagram (our results). (B) Metastable phase diagram obtained when the liquid mixture is heated over T_c.

stitution of some of sixfold coordinated Ga^{3+} by Ln^{3+} was checked with the experimental data obtained for the nonstoichiometry of the GGG. The theoretical data and experimental results are in close agreement, yielding information on the nonstoichiometry range of SmGG.

References

1. R. C. LINARES, *Solid State Commun.* **2,** 229 (1964).
2. C. D. BRANDLE, D. C. MILLER, AND J. W. NIELSEN, *J. Crystal Growth* **12,** 195 (1972).
3. C. D. BRANDLE AND A. J. VALENTINO, *J. Cryst. Growth* **12,** 3 (1972).
4. C. D. BRANDLE, *J. Cryst. Growth* **42,** 400 (1977).
5. D. M. HEINZ, L. A. MOUDY, P. E. ELKINS, AND D. J. KLEIN, *J. Electron Mater.* **1,** 319 (1972).
6. D. F. O'KANE, V. SADAGOPAN, AND E. A. GIESS, *J. Electrochem. Soc.* **120,** 9 (1973).
7. S. GELLER, *Z. Kristallogr.* **125,** 1 (1967); *Mater. Res. Bull.* **7,** 1219 (1972).
8. C. D. BRANDLE AND R. L. BARNS, *J. Cryst. Growth* **26,** 169 (1974).
9. M. ALLIBERT, C. CHATILLON, J. MARESCHAL, AND F. LISSALDE, *J. Cryst. Growth* **23,** 289 (1974).
10. M. A. DIGUISEPPE AND S. L. SOLED, *J. Solid State Chem.* **30,** 203 (1979).
11. M. A. DIGUISEPPE, S. L. SOLED, W. M. WENNER, AND J. E. MACUR, *J. Cryst. Growth* **49,** 746 (1980).
12. A. MAREZIO, J. P. REMEIKA, AND P. D. DERNIER, *Inorg. Chem.* **7,** 1337 (1968).
13. C. D. BRANDLE AND H. STEINFINK, *Inorg. Chem.* **8,** 1320 (1969).
14. J. WARSHAW AND R. ROY, *J. Amer. Ceram. Soc.* **42,** 434 (1959).
15. S. J. SCHNEIDER, R. S. ROTH, AND J. L. WARING, *J. Res. Nat. Bur. Stand. Sect. A* **65,** 345 (1961).
16. J. R. CARRUTHERS, M. KOKTA, R. L. BARNS, AND M. GRASSO, *J. Cryst. Growth* **19,** 204 (1973).
17. S. GELLER, P. J. CURLANDER, AND G. F. RUSE, *Mater. Res. Bull.* **9,** 637 (1974).
18. J. P. COUTURES, R. BERJOAN, G. BENEZECH, B. GRANIER, R. RENARD, AND M. FOEX, *Rev. Int. Hautes Temp. Refract.* **15,** 103 (1978).

19. J. P. COUTURES AND M. FOEX, *C. R. Acad. Sci. Paris Sér. C* **267,** 1577 (1968).

20. F. CABANNES, J. SIMONATO, M. FOEX, AND J. P. COUTURES, *High Temp.–High Pressures* **4,** 189 (1972).

21. J. COUTURES, E. ANTIC, G. SCHIFFMACHER, J. NICOLAS, AND J. P. COUTURES, *C.R. Acad. Sci. Ser. II* **296,** 347 (1983).

22. S. GELLER, *J. Chem. Phys.* **24,** 1236 (1956).

23. B. BOUDOT AND G. NURY, U.S. Patents 4-350 558, 4-350-559 (1982).

24. R. D. SHANNON AND C. T. PREWITT, *Acta Crystallogr. B* **25,** 965 (1969).

25. R. GILLISSEN, A. J. FLIPOT, AND R. LECOCQ, *J. Amer. Ceram. Soc.* **57,** 274 (1974).

26. J. L. CASLAVSKI AND D. J. VIECHNICKI, *J. Mater. Sci.* **15,** 1709 (1980).